

Manifold Characteristics That Predict Downstream Task Performance

Ruan van der Merwe¹ Gregory Newman¹ Etienne Barnard^{1,2}

Abstract

Pretraining methods are typically compared by evaluating the accuracy of linear classifiers, transfer learning performance, or visually inspecting the representation manifold’s (RM) lower-dimensional projections. We show that the differences between methods can be understood more clearly by investigating the RM directly, which allows for a more detailed comparison. To this end, we propose a framework and new metric to measure and compare different RMs. We also investigate and report on the RM characteristics for various pretraining methods. These characteristics are measured by applying sequentially larger local alterations to the input data, using white noise injections and Projected Gradient Descent (PGD) adversarial attacks, and then tracking each datapoint. We calculate the total distance moved for each datapoint and the relative change in distance between successive alterations. We show that self-supervised methods learn an RM where alterations lead to large but constant size changes, indicating a smoother RM than fully supervised methods. We then combine these measurements into one metric, the Representation Manifold Quality Metric (RMQM), where larger values indicate larger and less variable step sizes, and show that RMQM correlates positively with performance on downstream tasks.

1. Introduction

Understanding why deep neural networks generalise so well remains a topic of intense research, despite the practical successes that have been achieved with such networks. Less ambitiously than aiming for a complete understanding, we can search for characteristics that indicate good generalisation. Knowledge of such characteristics can then be incorporated into training methods and open more research

¹ByteFuse AI, Stellenbosch, South Africa ²Multilingual Speech Technologies, North-West University, South Africa. Correspondence to: Ruan van der Merwe <ruanh.vandermerwe@gmail.com>.

avenues. These characteristics can also be used to evaluate and compare networks.

Arguably the most successful current theories of generalisation focus on the flatness of the loss surface at the minima (Hochreiter & Schmidhuber, 1997; Dziugaite & Roy, 2017; Dherin et al., 2021) (even though the most straightforward measures of flatness are known to be deficient (Dinh et al., 2017)). (Petzka et al., 2021) expands on this argument and shows that these methods correlate strongly with model performance, and reflect the assumption that the labels are locally constant in feature space. A thorough survey by (Jiang et al., 2020) shows that some recent methods are, in fact, negatively correlated with generalisation.

To our knowledge, no theory looks at the structural characteristics of the learned Representation Manifold (RM) as a predictor for generalisation. We investigate whether structural characteristics in the RMs correlate with generalisation to task performance.

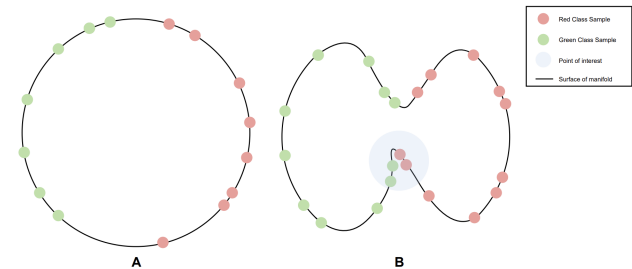


Figure 1. An illustration to give an intuitive understanding of why the structural characteristics of a RM should be considered a predictor of generalisation.

To illustrate the intuition behind our investigation, consider Figure 1, which represents two RMs, A and B. Assume that each RM is produced by the same architecture, trained on the same dataset; both have a flat minima but are trained with different methods. In the case of A, where the manifold is smooth, the sample representations of the Green class are, on average, closer to other Green class’s points. Likewise, presentations of the Red class will, on average, be closer to other Red class’s samples. On the other hand, if we consider RM B, there are chasms in the manifold that lead to some sample representations being closer to samples of the other

class rather than samples of their own class, as illustrated in the blue patch.

The purpose of this paper is to justify our claim that specific RM characteristics lead to generalisation. However, to do this, we must first define appropriate RM characteristics that reflect this intuition and show how to measure them.

Contribution: This paper aims to show with enough empirical evidence that looking at the representation manifold (RM) structure is a good research direction for explaining generalisation in deep learning structures. Following these strong empirical results, future work will require a deeper theoretical investigation into our findings. Our contributions in this paper can then be summarised as defining a model-agnostic and straightforward framework to measure RM characteristics. Using this framework, we compare the RMs learned by encoders trained using supervised, self-supervised and a mixture of both methods on the MNIST and CIFAR-10 datasets. We then present a new metric that calculates the quality of a manifold for generalisation, the Representation Manifold Quality Metric (RMQM). We show that this metric correlates strongly with downstream task performance. These observations support our intuition on the characteristics of an RM that lead to generalisation. We also release all code used in this project ¹.

2. Related Work

Representation learning Some of the earliest work in representation learning focused on pretraining networks by generating artificial labels from images and then training the network to predict these labels (Doersch et al., 2015; Zhang et al., 2016; Gidaris et al., 2018). Other techniques involve contrastive learning where representations from images are directly contrasted against one another such that the network learns to encode similar images to similar representations (Schroff et al., 2015; Oord et al., 2018; Chen et al., 2020; He et al., 2020; Le-Khac et al., 2020).

Comparing representations from trained neural networks (Yamins et al., 2014; Cadena et al., 2019) compares how similar representations are by linearly regressing over the one representation to predict the other representation. The R^2 coefficient is then used as a metric to quantify similarity. This metric is not symmetric. Symmetrical methods compare representations from different neural networks by creating a similarity matrix between the hidden representations of all layers as was done in (Laakso & Cottrell, 2000; Kriegeskorte et al., 2008; Li et al., 2016; Wang et al., 2018; Kornblith et al., 2019).

Manifold Learning The Manifold Hypothesis states that

¹<https://github.com/ByteFuse/representation-manifold-quality-metric>

practical high dimensional datasets lie on a much lower dimensional manifold (Carlsson et al., 2008; Fefferman et al., 2016; Goodfellow et al., 2016). Manifold learning techniques aim to learn this lower-dimensional manifold by performing non-linear dimensionality reduction. A typical application of these non-linear reductions is visualising high dimensional data in two-dimensional or three-dimensional settings. Popular techniques include (Tenenbaum et al., 2000; Van der Maaten & Hinton, 2008; McInnes et al., 2018). These techniques have been used in various studies to compare different learned representation manifolds (Chen et al., 2019; van der Merwe, 2020; Li et al., 2020; Liu et al., 2022).

Comparing manifolds To evaluate the performance of Generative Adversarial Networks, (Barannikov et al., 2021) introduces the Cross-Barcode tool that measures the differences in topologies between two manifolds, which they approximate by the sampled data points from the underlying data distributions. They then derive the Manifold Topology Divergence, based on the sum of the lengths of segments in the Cross-Barcode. (Zhou et al., 2021) also evaluates generative models by quantifying representation disentanglement. They do this by measuring the topological similarity of conditional submanifolds from the latent space. (Shao et al., 2018) investigates the Riemannian geometry of latent manifolds, specifically the curvature of the manifolds. They conclude that having latent coordinates that approximate geodesics is a desirable property of latent manifolds. To our knowledge, there has not been a study done on measuring the manifold’s structural characteristics based on small local alterations to the input data, applied to non-generative encoders.

Predictors of generalisation (Jiang et al., 2020) performed a large scale study of generalisation in deep learning, and we refer the reader to this work for a well-documented review. To our knowledge there has been no work done on using the structure of the RM as a predictor of generalisation.

3. Approach

Describing all the details of a high-dimensional representation manifold (RM) is an impossible task; we can at best strive to find characteristics that summarise salient properties of the RM. When measuring these characteristics, one will therefore have a discrete view of the RM (Barannikov et al., 2021), made out of the predicted representations from the input data. We propose measuring individual distance metrics for each representation of an input sample relative to representations of data close to it.

By staying in the neighbourhood of each representation, we can measure the surface surrounding that point using standard distance metrics, effectively walking on the local structure and measuring the size of each step relative to the

change in input. By inspecting all these locally measured structures together, one describes the structure for the entire RM in terms of its local stability.

The caveat is that one requires representations in close proximity on the RM to do these measurements. However, practical RMs have many dimensions, implying that data points tend to be well separated, even if they originate from the same underlying class (Bárány & Füredi, 1988; Balestrierio et al., 2021). We thus need to create these proximate representations artificially.

We do this by applying sequentially larger local alterations to the input data and computing the resulting representations. By increasing the size of the alteration, we step further on the RM surface and thus measure characteristics further away but still local for the magnitude of changes that we employ.

Next we will discuss the alteration methods we employ and the local characteristics we measure.

3.1. Alteration Methods

Let an RM be represented by $\phi_\theta = f_\theta(\mathbf{X})$, where f_θ is a feature extractor parameterised by θ and \mathbf{X} is a data set (e.g. input images). With A representing a function that applies small local alterations to pixels in the image, each altered data point projected down to the RM is represented as $\phi_{\theta,i} = f_\theta(A_j(x_i))$, where $x_i \in \mathbf{X}$ and A_j the j th iteration of the alteration function.

The two alteration methods we use in our experiments are the same methods (Hoffman et al., 2019) used to evaluate the robustness of a Jacobian regulariser. We chose these methods because they result in either random local alterations or guided alteration, thus giving us different paths on the RM to evaluate.

White noise injection Here we alter each input image x_i by adding an alteration vector randomly, a , with components independently drawn from a normal distribution with variance ϵ^2 , thus $a \sim \mathcal{N}(0, \epsilon^2)$. In order to increase the alteration strength, we increase ϵ from zero to one with 100 in equal steps, indexed by j . Thus, alteration j for datapoint x_i is given by $x_{ij} = [x_i + a_j]_{clip}$, where $a_j \sim \mathcal{N}(0, \epsilon_j^2)$ and $[\cdot]_{clip}$ clips the image to be between zero and one.

PGD attack Whereas white noise injections will allow us to walk on the surface of an RM in random directions, altering the image in a way that deliberately aims to fool the trained function f_θ will allow us to walk in a direction influenced by decision boundaries on the RM. In this paper we will implement an extension of fast gradient sign method (FGSM) (Goodfellow et al., 2015), namely projected gradient descent (PGD) (Madry et al., 2018). FGSM consists of adding a vector to the original image, where this vector

consists of the sign of the gradient for the loss functions with respect to the input image, scaled by a value ϵ_{FGSM} . PGD iterates this process for several iterations. Calculating the j th alteration of x_i , represented by $x_{i,j}$ can be defined as

$$x_{i,j} = [x_{i,j-1} + \epsilon_{FGSM} \cdot (\nabla_{x_{i,j-1}} \mathcal{L}(\theta, x_{i,j-1}, y))]_{clip} \quad (1)$$

where \mathcal{L} is the loss function for the relevant training method.

Given that the original target for these adversarial attacks was a network that classifies images. In order to then apply PGD attack to the triplet variants, we calculate the loss precisely as usual and then calculate the gradient with regards to the anchor image. When calculating the gradient for NT-XENT methods, we compare a non-augmented image with an augmented version and then calculate the gradient with respect to the unaugmented image. We apply the PGD attack for 30 iterations and save each iteration, with $\epsilon_{FGSM} = 2/255$.

3.2. Manifold Characteristics

Let A_j be the j th iteration of an alteration method, where each successive iteration employs a stronger alteration. Also, let $\phi_{i,j}$ be the projected point on the RM produced by $f(A_j(x_i))$, where $x_i \in \mathbf{X}$.

Average distance moved The first characteristic we measure is the total of the normalised Euclidean distances between the original point, $\phi_{i,0}$, and each altered point, $\phi_{i,j}$. The average distance moved for image x_i is represented as $\frac{1}{J} \sum_j \|\phi_{i,0} - \phi_{i,j}\|_2$, where we can then average over each point to find the average distance moved for a given RM and alteration. Finally, the average over images is

$$D(\phi, A) = \frac{1}{NJ} \sum_i^N \sum_j^J \|\phi_{i,0} - \phi_{i,j}\|_2 \quad (2)$$

where N is the number of images considered and J is the number of alterations. $D(\phi, A)$ thus indicates how robust the RM is to alterations A .

Average distance spikes We also measure the relative change in distance between successive alterations. These relative distance changes are measured both with respect to the original representation and relative to each previous alteration. We average the magnitudes of these changes as we are not interested in the direction of the change to gauge how smooth an RM is. To understand how relative changes relate to smoothness, recall that we only apply alterations that keep us close to the given data points. Therefore, we can only have big spikes if the RM contains significant chasms or bumps (small alterations in input data should result in constant distance increases if the RM is smooth).

In order to calculate these relative changes for a single representation, refer to Equation (3) which calculates the relative

change according to the original representation, D_{RC} and Equation (4) which calculates the relative change according to the distance between the previous alterations P_{RC} . In both equations, $d(\cdot)$ is a distance function. In order to get the overall metrics, we average the values over all data points.

$$D(\phi_i, A)_{RC} = \frac{1}{J} \sum_{j=1}^J \left| \frac{d(\phi_{i,0}, \phi_{i,j}) - d(\phi_{i,0}, \phi_{i,j-1})}{d(\phi_{i,0}, \phi_{i,j})} \right| \quad (3)$$

$$P(\phi_i, A)_{RC} = \frac{1}{J} \sum_{j=2}^J \left| \frac{d(\phi_{i,j-1}, \phi_{i,j}) - d(\phi_{i,j-1}, \phi_{i,j-2})}{d(\phi_{i,j-1}, \phi_{i,j})} \right| \quad (4)$$

4. Comparing Different Training Methods

We now measure the characteristics defined in Section 3 for five different training methods, applied to two different encoders and data sets. By comparing these five methods, we discover common properties for related methods, thereby gaining a better understanding of the learned RMs.

The first method we investigate employs encoders trained with vanilla supervised learning with Cross-Entropy loss, where we then take the second to last layer output as the representations. We also use the SimCLR method introduced in (Chen et al., 2020). This method compares two augmented versions of the same image and brings their representations closer together using the Normalised Temperature-scaled Cross-Entropy (NT-XENT) Loss (Sohn, 2016). Along with this, we trained encoders using two different implementations of Triplet-Loss (Weinberger et al., 2006; Schroff et al., 2015). We believe these techniques represent the major families of training techniques and provide enough information on how different techniques learn different RM structures. We propose that a full-scale investigation be performed on most training techniques found in current literature, in a future paper.

We mine the triplets in a supervised manner for the first implementation using the image labels. We apply the SimCLR method for the second implementation, replacing NT-XENT with Triplet loss. We refer to the former method as Triplet-Supervised going forward and the latter as Triplet-SS. We do this to see the effect of the indirect supervised signal on the method. Lastly, to see the effect of directly combining a contrastive signal with a supervised signal, we combine Triplet-Loss with Cross-Entropy loss as was also done in (van der Merwe, 2020). Here the second to last layer’s outputs are fed into the Triplet-Loss function, where the triplets are mined using the same labels used for the Cross-Entropy loss which takes as input the logits produced by the last layer.

We apply these methods to an altered version of the LeNet-5 architecture introduced in (LeCun et al., 1998), trained on the MNIST data set (LeCun et al., 1998) and a Resnet-18 (He et al., 2016) trained on the CIFAR-10 data set (Krizhevsky et al., 2009).

We train our encoders with six different embedding sizes, ranging from 16 to 512 in powers of two. We also train with two different optimisers, namely Stochastic Gradient Descent (SGD) with Nesterov Momentum (Sutskever et al., 2013) and Adam (Kingma & Ba, 2015).

For SGD with Nesterov momentum, we set the learning rate to 0.001 and momentum to 0.9. Our learning rate is also 0.001 with the default PyTorch hyperparameters for Adam. We train the CIFAR-10 encoders for 100 epochs and the MNIST encoders for seven epochs.

To ensure that each RM can be compared fairly to each other, all image alterations are exactly the same for each method when calculating the manifold characteristics. We report in the rest of this section using the average results over both the Adam and SGD trained encoders, as the results were similar for both.

4.1. Measuring Distances

Figure 2 shows the average normalised Euclidean distance to the original MNIST digits as we increase the amount of alteration applied to each digit.

Here, A is the white noise injection alteration. As the embedding dimension increases, the self-supervised methods move further from the original point than the supervised signal methods. We also notice that the Cross-Entropy encoder’s average distance away from the original representation stays very low, with the Triplet-Entropy and Triplet-Supervised encoders falling in between. We suspect this is because they contain both supervised and unsupervised signals in the training process.

When A is the PGD attack, we see the same pattern emerging for the CIFAR-10 encoders, shown in Figure 3. Here though, we can see a much more significant difference between self-supervised methods and methods containing a supervised signal: the NT-XENT and Triplet-SS measurements grow to have much larger values.

In Table 1 we summarise the D values, which is calculated using Equation (2), for the MNIST encoders. We average over embedding dimensions and calculate the standard deviation for each method. The common trend among both alteration methods is that NT-XENT and Triplet-SS alterations always move farther away from the original representation than the other methods. We can also see that the total distance moved decreases from self-supervised to pure supervised learning methods.

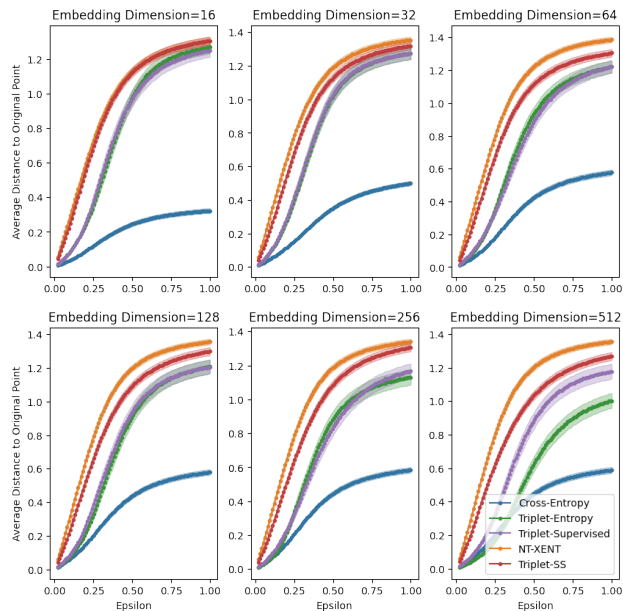


Figure 2. The normalised Euclidean distance between the original MNIST digit and the same digit altered by our white noise injection method. We perform this measurement for each embedding dimension and digit in the test set. We then calculate the standard error shown with the mean results.

These results indicate that the encoder is more robust to minor perturbations (as measured by the distance moved from the original image) if the training method contains a strong supervised signal.

4.2. Measuring Spikes

Following the same steps as in Section 4.1, we now study the relative change in distances measured. The relative change in distance to the original representation, plotted against the amount of PGD attack iterations, is shown in Figure 4.

We see a reversal of the graphs in Section 4.1: the self-supervised methods start with high relative changes which decrease rapidly. Methods containing a supervised signal have larger spikes and error bands. All this indicates a less smooth journey in the RM between alterations for the supervised methods.

The same trend is present for CIFAR-10 models when we inject white noise. Here though, the Triplet-Supervised method is unstable for several values of the embedding dimension, whereas the NT-XENT and Triplet-SS again have the smallest spikes.

Table 2 shows the overall average values for each spike metric for each method. NT-XENT and Triplet-SS have the smallest spikes for both forms of alteration, whereas

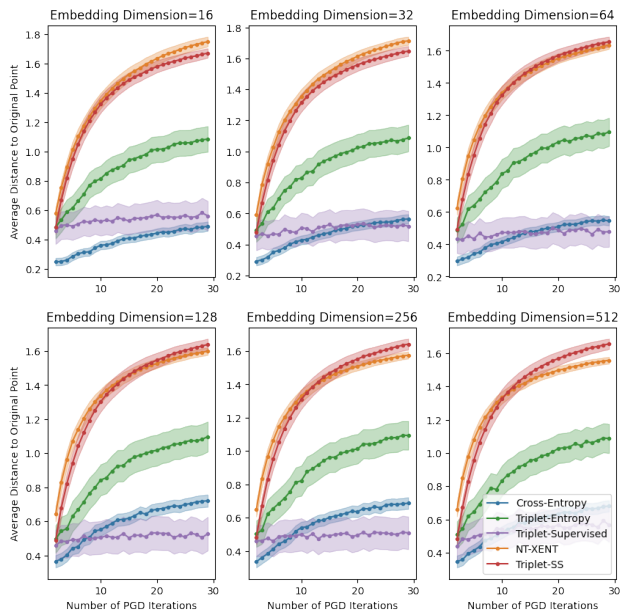


Figure 3. The normalised Euclidean distance between the original CIFAR-10 image and the same image altered by sequential PGD attack iterations.

Table 1. The average distance each points moves relative to the original point for both the white noise injection and PGD Attack alterations for the MNIST encoders. The results are averaged over both the embedding dimension of an encoder and the optimiser used.

METHOD	NOISE	PGD
CROSS-ENTROPY	0.33 ± 0.15	0.21 ± 0.08
TRIPLET-ENTROPY	0.73 ± 0.11	0.33 ± 0.08
TRIPLET-SUPERVISED	0.77 ± 0.06	0.38 ± 0.10
TRIPLET-SS	0.93 ± 0.13	0.66 ± 0.17
NT-XENT	1.01 ± 0.04	0.68 ± 0.10

Triplet-Supervised results in very non-smooth RMs.

Self-supervised methods therefore learn structures in which a step in most directions, at most locations, induces steps of similar size on the RM. That is, these self-supervised methods have smoother RMs than the other methods.

5. Representation Manifold Quality Metric

In Section 4 we showed empirically that an RM learned by self-supervised methods has a structure that has the following property: When moving in any direction on the surface of RM, it will result in a relatively large displacement, but these displacements are on average the same size no matter where or in what direction a step is taken. The opposite is true with methods containing a supervised signal: moving

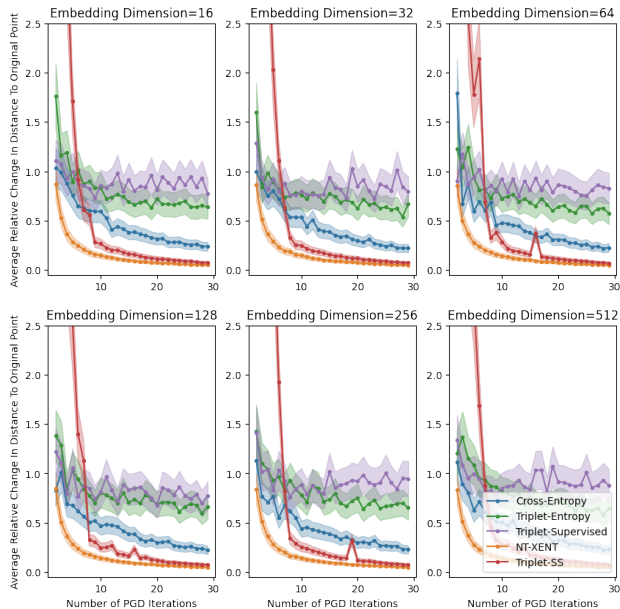


Figure 4. The relative change in distance to the original point, plotted against the number of PGD iterations for the encoders trained on the MNIST dataset.

in the surface results in smaller displacements, but those displacements are significantly more variable in size.

In order to determine which of these two groups of characteristics are more desirable for downstream tasks, we combine these characteristics into one metric, the Representation Manifold Quality Metric (RMQM).

With this single metric describing an RM, we can perform various downstream tasks with our encoders and see how the performance correlates with the value of the RMQM. We define the RMQM as

$$RMQM = \ln(1 + D + D_{PC}^{-1} + P_{PC}^{-1}) \quad (5)$$

Here D is the average distance moved measured relative to the original representation, D_{PC} is the relative change in distance between each subsequent alteration and the original representation and P_{PC} is the relative change of the distances between altered representations, as defined in Equations (2) to (4).

We apply the natural logarithm to scale the values, and we add one to ensure we do not have any negative values.

Thus, RMQM is designed to yield large values for relatively smooth RMs with relatively large sensitivity to changes in the input. Below, we only interpret the RMQM score when A is the white noise injection alteration, since the method dependence of the PGD alterations complicates our ability to compare the various methods.

Table 2. The average change in the distance each point moves relative to the original point, compared against the previous alteration’s distance. Results are calculated for both the white noise injection and PGD Attack alterations for the CIFAR-10 encoders. The results are averaged over both the embedding dimension of an encoder and the optimiser used.

METHOD	NOISE	PGD
CROSS-ENTROPY	0.11 ± 0.03	0.34 ± 0.04
TRIPLET-ENTROPY	0.18 ± 0.04	0.89 ± 0.35
TRIPLET-SUPERVISED	0.86 ± 0.85	2.97 ± 1.61
TRIPLET-SS	0.06 ± 0.01	0.06 ± 0.04
NT-XENT	0.04 ± 0.01	0.10 ± 0.01

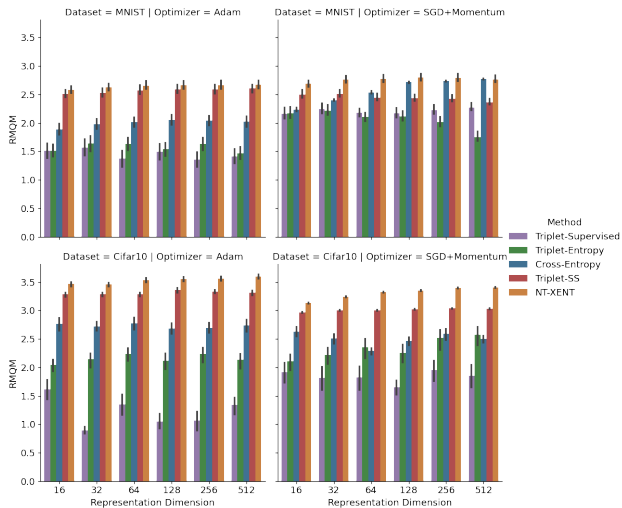


Figure 5. RMQM for white noise injections, over every embedding dimension for each encoder.

In Figure 5 we show the RMQM score for each of our encoders, with A being white noise injections. For the MNIST encoders trained using SGD and Nesterov momentum, as the embedding size increases, the RMQM for Cross-Entropy overtakes Triplet-SS, indicating that the RM is more similar in this setup to one produced by NT-XENT trained encoders. In the other cases, there is an overall trend for the NT-XENT and Triplet-SS encoders to have the highest RMQM, followed by Cross-Entropy and then lastly, Triplet-Entropy and Triplet-Supervised.

5.1. Correlation between RMQM and Downstream Tasks.

In order to find what RM characteristics are desirable, we measure how RMQM correlates with downstream task performance. If we find a strong positive correlation, an RM with a smooth structure and large displacements is desirable. If there is a strong negative correlation, then an RM

that contains chasms and bumps and small displacements is desirable.

We define the task performance as the normalised test accuracy of a K-Nearest Neighbour (KNN) model, with only one nearest neighbour ($K = 1$), trained on the representations created by the encoder. We believe this is an appropriate measure of task performance as most use cases today utilise representations to perform vector search and KNN model’s accuracy is a good approximation of this task. We believe this is a valid task for performance measurement, as this task does not change the learned RM structure, as would be the case when fine-tuning the encoders on a new dataset with Cross-Entropy. The MNIST encoders will be tested on the OMNIGLOT (Lake et al., 2015) and the KMNIST (Clanuwat et al., 2018) datasets, with the CIFAR-10 encoders being tested on the Caltech-101 (Fei-Fei et al., 2004) and CIFAR-100 (Krizhevsky et al., 2009) datasets. We believe these datasets provide a large enough semantic gap towards the original datasets, as we do not measure for extreme generalisation to any dataset.

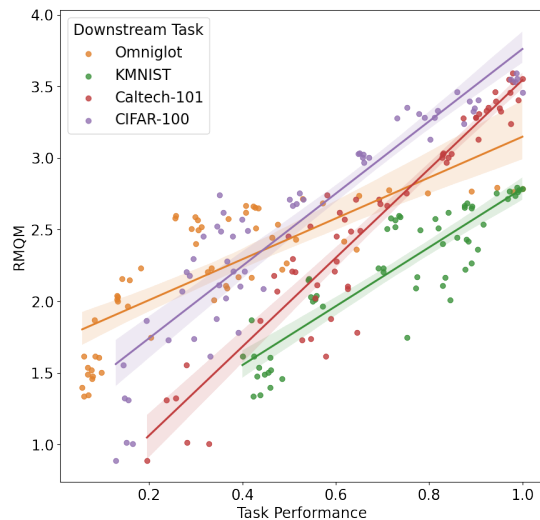


Figure 6. RMQM versus downstream task performance. The dots represent each encoder’s performance and RMQM score, colour coded by task. As one can see, there is a strong positive correlation between RMQM and downstream task performance.

Figure 6 represents RMQM versus downstream task performance. We also show the correlations between RMQM, downstream task performance and embedding dimensions in Table 3. What is clear from both Figure 6 and Table 3 is that there is a strong positive correlation (0.75) between RMQM and downstream task performance, whereas RMQM and

downstream task performance are practically uncorrelated with the embedding dimension of the encoders. This justifies our statement that RM characteristics are essential and not simply the number of features learned by an encoder.

That is, when vector search is the downstream task performance, an encoder that learned an RM with smooth structure and large displacements will tend to perform well on downstream search tasks.

Table 3. The overall correlation coefficients between RMQM, downstream task performance and embedding dimension.

	TASK PERFORMANCE	RMQM
RMQM	0.75	1
DIMENSION	0.096	0.026

To help better understand these perhaps unintuitive results, consider the case when we calculate the RMQM using white noise alterations. Take the MNIST encoders as an example, and consider a specific MNIST image (any digit). When applied to this digit, there exists a random vector that will transform it into one of the Omniglot characters. In general, the variants of this Omniglot character will differ from that digit image by similar noise vectors. Thus when we encode this Omniglot character image and its variants using a self-supervised trained encoder, the KNN models can accurately identify new images, because from the perspective of the RM, these new characters correspond to the noise-altered version of our original MNIST digit. On the RM then, this new character and its variants are projected with a similar step size away from the original MNIST digit. Due to the similar noise vector added, these projections are also in a similar direction. These projected characters are also close because there are few chasms or bumps a projection can land on, allowing a nearest neighbour search to perform well.

6. Conclusion

We propose a framework to measure the characteristics of learned representation manifolds (RM). We measure the characteristics by applying sequentially stronger local alterations to the input data and measuring how these altered representations move relative to the original representation and the successive alterations. We show that self-supervised learning methods learn RMs in which motion in any direction on the surface will result in relatively large displacements. However, these displacements are relatively similar no matter where or in what direction a step is taken.

To identify RM characteristics related to good downstream task performance, we combine our measurements into a single metric, the Representation Manifold Quality Metric (RMQM). RMQM is designed to yield large values for

relatively smooth RMs with relatively large sensitivity to changes in the input. We then measure the downstream task performance for several tasks and find a strong positive correlation with RMQM. This strong correlation indicates that the structure of a learned manifold is another strong predictor for the generalisation of neural networks. This also shows that self-supervised methods lead to state-of-the-art performance due to the underlying RM structure, which is sensitive to alterations in the input, utilising a relatively smooth manifold.

References

- Balestriero, R., Pesenti, J., and LeCun, Y. Learning in high dimension always amounts to extrapolation. *arXiv preprint arXiv:2110.09485*, 2021.
- Barannikov, S., Trofimov, I., Sotnikov, G., Trimbach, E., Korotin, A., Filippov, A., and Burnaev, E. Manifold topology divergence: a framework for comparing data manifolds. In Beygelzimer, A., Dauphin, Y., Liang, P., and Vaughan, J. W. (eds.), *Advances in Neural Information Processing Systems*, 2021. URL <https://openreview.net/forum?id=Fj6kQJbHwM9>.
- Bárány, I. and Füredi, Z. On the shape of the convex hull of random points. *Probability theory and related fields*, 77(2):231–240, 1988.
- Cadena, S. A., Sinz, F. H., Muhammad, T., Froudarakis, E., Cobos, E., Walker, E. Y., Reimer, J., Bethge, M., Tolia, A., and Ecker, A. S. How well do deep neural networks trained on object recognition characterize the mouse visual system? 2019.
- Carlsson, G., Ishkhanov, T., De Silva, V., and Zomorodian, A. On the local behavior of spaces of natural images. *International journal of computer vision*, 76(1):1–12, 2008.
- Chen, T., Kornblith, S., Norouzi, M., and Hinton, G. E. A simple framework for contrastive learning of visual representations. In *Proceedings of the 37th International Conference on Machine Learning, ICML 2020, 13-18 July 2020, Virtual Event*, volume 119 of *Proceedings of Machine Learning Research*, pp. 1597–1607. PMLR, 2020. URL <http://proceedings.mlr.press/v119/chen20j.html>.
- Chen, Z.-M., Wei, X.-S., Wang, P., and Guo, Y. Multi-label image recognition with graph convolutional networks. In *Proceedings of the IEEE Conference on Computer Vision and Pattern Recognition (CVPR)*, pp. 5177–5186, 2019.
- Clanuwat, T., Bober-Irizar, M., Kitamoto, A., Lamb, A., Yamamoto, K., and Ha, D. Deep learning for classical japanese literature. *ArXiv*, abs/1812.01718, 2018.
- Dherin, B., Munn, M., and Barrett, D. G. The geometric occam’s razor implicit in deep learning. *arXiv preprint arXiv:2111.15090*, 2021.
- Dinh, L., Pascanu, R., Bengio, S., and Bengio, Y. Sharp minima can generalize for deep nets. In Precup, D. and Teh, Y. W. (eds.), *Proceedings of the 34th International Conference on Machine Learning (ICML)*, volume 70 of *Proceedings of Machine Learning Research*, pp. 1019–1028. PMLR, 2017. URL <http://proceedings.mlr.press/v70/dinh17b.html>.
- Doersch, C., Gupta, A., and Efros, A. A. Unsupervised visual representation learning by context prediction. In *2015 IEEE International Conference on Computer Vision, ICCV*, pp. 1422–1430. IEEE Computer Society, 2015. URL <https://doi.org/10.1109/ICCV.2015.167>.
- Dziugaite, G. K. and Roy, D. M. Computing nonvacuous generalization bounds for deep (stochastic) neural networks with many more parameters than training data. In Elidan, G., Kersting, K., and Ihler, A. T. (eds.), *Proceedings of the Thirty-Third Conference on Uncertainty in Artificial Intelligence, UAI*. AUAI Press, 2017. URL <http://auai.org/uai2017/proceedings/papers/173.pdf>.
- Fefferman, C., Mitter, S., and Narayanan, H. Testing the manifold hypothesis. *Journal of the American Mathematical Society*, 29(4):983–1049, 2016.
- Fei-Fei, L., Fergus, R., and Perona, P. Learning generative visual models from few training examples: An incremental bayesian approach tested on 101 object categories. In *CVPR Workshops*, 2004.
- Gidaris, S., Singh, P., and Komodakis, N. Unsupervised representation learning by predicting image rotations. In *6th International Conference on Learning Representations, ICLR*. OpenReview.net, 2018. URL <https://openreview.net/forum?id=Slv4N2l0->.
- Goodfellow, I., Bengio, Y., and Courville, A. *Deep learning*. MIT press, 2016.
- Goodfellow, I. J., Shlens, J., and Szegedy, C. Explaining and harnessing adversarial examples. In Bengio, Y. and LeCun, Y. (eds.), *3rd International Conference on Learning Representations, ICLR*, 2015. URL <http://arxiv.org/abs/1412.6572>.
- He, K., Zhang, X., Ren, S., and Sun, J. Deep residual learning for image recognition. In *Proceedings of the IEEE conference on computer vision and pattern recognition (CVPR)*, pp. 770–778, 2016. URL <https://doi.org/10.1109/CVPR.2016.90>.

- He, K., Fan, H., Wu, Y., Xie, S., and Girshick, R. B. Momentum contrast for unsupervised visual representation learning. In *IEEE/CVF Conference on Computer Vision and Pattern Recognition CVPR*, pp. 9726–9735. Computer Vision Foundation / IEEE, 2020. URL <https://doi.org/10.1109/CVPR42600.2020.00975>.
- Hochreiter, S. and Schmidhuber, J. Flat Minima. *Neural Computation*, 9(1):1–42, 1997. ISSN 0899-7667. doi: 10.1162/neco.1997.9.1.1. URL <https://doi.org/10.1162/neco.1997.9.1.1>.
- Hoffman, J., Roberts, D. A., and Yaida, S. Robust learning with jacobian regularization. *ArXiv*, abs/1908.02729, 2019.
- Jiang, Y., Neyshabur, B., Mobahi, H., Krishnan, D., and Bengio, S. Fantastic generalization measures and where to find them. 2020. URL <https://openreview.net/forum?id=SJgIPJBFvH>.
- Kingma, D. P. and Ba, J. Adam: A method for stochastic optimization. In *3rd International Conference on Learning Representations, (ICLR)*, 2015. URL <http://arxiv.org/abs/1412.6980>.
- Kornblith, S., Norouzi, M., Lee, H., and Hinton, G. E. Similarity of neural network representations revisited. In Chaudhuri, K. and Salakhutdinov, R. (eds.), *Proceedings of the 36th International Conference on Machine Learning (ICML)*, volume 97 of *Proceedings of Machine Learning Research*, pp. 3519–3529. PMLR, 2019. URL <http://proceedings.mlr.press/v97/kornblith19a.html>.
- Kriegeskorte, N., Mur, M., and Bandettini, P. A. Representational similarity analysis-connecting the branches of systems neuroscience. *Frontiers in systems neuroscience*, 2:4, 2008.
- Krizhevsky, A. et al. Learning multiple layers of features from tiny images. Technical report. 2009.
- Laakso, A. and Cottrell, G. Content and cluster analysis: assessing representational similarity in neural systems. *Philosophical psychology*, 13(1):47–76, 2000.
- Lake, B. M., Salakhutdinov, R., and Tenenbaum, J. B. Human-level concept learning through probabilistic program induction. *Science*, 350(6266):1332–1338, 2015.
- Le-Khac, P. H., Healy, G., and Smeaton, A. F. Contrastive representation learning: A framework and review. *IEEE Access*, 8:193907–193934, 2020. URL <https://doi.org/10.1109/ACCESS.2020.3031549>.
- LeCun, Y., Bottou, L., Bengio, Y., and Haffner, P. Gradient-based learning applied to document recognition. volume 86, pp. 2278–2324. Ieee, 1998.
- Li, X., Yin, X., Li, C., Zhang, P., Hu, X., Zhang, L., Wang, L., Hu, H., Dong, L., Wei, F., et al. Oscar: Object-semantic aligned pre-training for vision-language tasks. In *European Conference on Computer Vision (ECCV)*, pp. 121–137. Springer, 2020.
- Li, Y., Yosinski, J., Clune, J., Lipson, H., and Hopcroft, J. E. Convergent learning: Do different neural networks learn the same representations? In *4th International Conference on Learning Representations, ICLR*, 2016. URL <http://arxiv.org/abs/1511.07543>.
- Liu, D., Qu, X., Wang, Y., Di, X., Zou, K., Cheng, Y., Xu, Z., and Zhou, P. Unsupervised temporal video grounding with deep semantic clustering. *arXiv preprint arXiv:2201.05307*, 2022.
- Madry, A., Makelov, A., Schmidt, L., Tsipras, D., and Vladu, A. Towards deep learning models resistant to adversarial attacks. In *6th International Conference on Learning Representations, ICLR*, 2018. URL <https://openreview.net/forum?id=rJzIBfZAb>.
- McInnes, L., Healy, J., and Melville, J. Umap: Uniform manifold approximation and projection for dimension reduction. *arXiv preprint arXiv:1802.03426*, 2018.
- Oord, A. v. d., Li, Y., and Vinyals, O. Representation learning with contrastive predictive coding. *arXiv preprint arXiv:1807.03748*, 2018.
- Petzka, H., Kamp, M., Adilova, L., Sminchisescu, C., and Boley, M. Relative flatness and generalization. *Advances in Neural Information Processing Systems*, 34, 2021.
- Schroff, F., Kalenichenko, D., and Philbin, J. Facenet: A unified embedding for face recognition and clustering. In *Proceedings of the IEEE Conference on Computer Vision and Pattern Recognition (CVPR)*, pp. 815–823, 2015. URL <https://doi.org/10.1109/CVPR.2015.7298682>.
- Shao, H., Kumar, A., and Fletcher, P. T. The riemannian geometry of deep generative models. In *2018 IEEE Conference on Computer Vision and Pattern Recognition Workshops, CVPR Workshops 2018, Salt Lake City, UT, USA, June 18-22, 2018*, pp. 315–323. Computer Vision Foundation / IEEE Computer Society, 2018.
- Sohn, K. Improved deep metric learning with multi-class n-pair loss objective. In Lee, D. D., Sugiyama, M., von Luxburg, U., Guyon, I., and Garnett, R. (eds.), *Advances in Neural Information Processing Systems*, pp. 1849–1857, 2016.
- Sutskever, I., Martens, J., Dahl, G., and Hinton, G. On the importance of initialization and momentum in deep

- learning. In *Proceedings of the 30th International Conference on Machine Learning (ICML)*, pp. 1139–1147, 2013. URL <https://proceedings.mlr.press/v28/sutskever13.html>.
- Tenenbaum, J. B., De Silva, V., and Langford, J. C. A global geometric framework for nonlinear dimensionality reduction. *science*, 290(5500):2319–2323, 2000.
- Van der Maaten, L. and Hinton, G. Visualizing data using t-sne. *Journal of machine learning research*, 9(11), 2008.
- van der Merwe, R. Triplet entropy loss: Improving the generalisation of short speech language identification systems. *arXiv preprint arXiv:2012.03775*, 2020.
- Wang, L., Hu, L., Gu, J., Hu, Z., Wu, Y., He, K., and Hopcroft, J. E. Towards understanding learning representations: To what extent do different neural networks learn the same representation. pp. 9607–9616, 2018.
- Weinberger, K. Q., Blitzer, J., and Saul, L. Distance metric learning for large margin nearest neighbor classification. In Weiss, Y., Schölkopf, B., and Platt, J. (eds.), *Advances in Neural Information Processing Systems*, volume 18. MIT Press, 2006. URL <https://proceedings.neurips.cc/paper/2005/file/a7f592cef8b130a6967a90617db5681b-Paper.pdf>.
- Yamins, D. L., Hong, H., Cadieu, C. F., Solomon, E. A., Seibert, D., and DiCarlo, J. J. Performance-optimized hierarchical models predict neural responses in higher visual cortex. *Proceedings of the national academy of sciences*, 111(23):8619–8624, 2014.
- Zhang, R., Isola, P., and Efros, A. A. Colorful image colorization. In Leibe, B., Matas, J., Sebe, N., and Welling, M. (eds.), *Computer Vision - ECCV 2016 - 14th European Conference*, volume 9907 of *Lecture Notes in Computer Science*, pp. 649–666. Springer, 2016.
- Zhou, S., Zelikman, E., Lu, F., Ng, A. Y., Carlsson, G. E., and Ermon, S. Evaluating the disentanglement of deep generative models through manifold topology. In *9th International Conference on Learning Representations, ICLR*. OpenReview.net, 2021. URL https://openreview.net/forum?id=djwS0m4Ft_A.